Structure of Self-Excited Oscillations in Transonic Diffuser Flows

T. J. Bogar*
McDonnell Douglas Corporation, St. Louis, Missouri

Two-component laser Doppler velocimeter (LDV) measurements were made in a supercritical, separated, transonic diffuser flow exhibiting self-excited oscillations. The velocity data were ensemble-averaged with respect to the shock oscillation phase, and maps of various flow quantities were generated. The time evolution of the fluctuating velocity field shows a large, rotating structure that originates near the upstream edge of the separation bubble and is convected downstream. The streamwise velocity fluctuation pattern for the self-excited oscillations resembles the oscillation pattern that occurs when the flow is mechanically excited at the downstream end. Velocity fluctuations calculated from ensemble-averaged core total and static pressure data show good agreement with the LDV data.

Nomenclature

f = frequency
t = time
u, U = streamwise velocity component, amplitude of first Fourier component of ensemble-averaged streamwise velocity component
v = transverse velocity component
x = streamwise coordinate ($x=0$ at throat, positive streamwise)
y = vertical (transverse) coordinate ($y=0$ at lower wall, positive upward)
z = spanwise coordinate (defined by right-handed system with x and y)
δ^* = displacement thickness
ϕ = phase relative to shock oscillation phase

Subscripts

m = midstream ($y=0.432$, core probe height)
s = static
σ = shock
0 = plenum

Superscripts

$(\tilde{\ })$ = length normalized by throat height
$(\ )'$ = time-dependent component

Introduction

SUPERSONIC aircraft and missile inlets may exhibit self-sustained oscillations (dynamic distortion, buzz) which constitute major limitations in off-design vehicle performance.[1-3] Sufficiently severe distortion in turbojet systems can lead to compressor stall and blade fatigue; buzz leads to high periodic structural loads and drastically decreased mass flow through the propulsion system, causing a major loss of thrust. A common remedy is to design the propulsion systems with a sufficient safety margin, at the expense of cruise operating characteristics, such that flow unsteadiness induced by sharp maneuvers, wind gusts, and the like will not lead to instabilities. The amount of margin required is estimated, or determined through costly wind tunnel tests; often the result is overspecification, which penalizes cruise performance excessively. To satisfactorily accommodate the self-sustained oscillations during system design, a thorough understanding of the oscillations is required.

The engine or combustor to which the inlet is attached may generate its own oscillations, as in the case of dump-combustor ramjets.[4-7] Resonant coupling between the combustor and inlet could cause unacceptably high pressure oscillations, adversely affecting propulsion system performance.[8,9] Knowledge of the origin of inlet oscillations can allow an assessment of the degree to which such coupling will occur.

Studies conducted over the past several years at McDonnell Douglas Research Laboratories have employed a variety of transonic diffusers (supercritically operated convergent-divergent channels) to model inlet flows.[10-14] The dominant features of supercritically operated supersonic inlet flows are a normal-shock/boundary-layer interaction and the decelerating subsonic channel flow downstream of the interaction. Transonic diffusers contain such a flow pattern and, therefore, properly simulate inlets for research purposes. (Subcritical inlet flows, which are significantly influenced by the presence of leading edges, are not simulated by this approach.) Rather than attempting to duplicate a specific operational inlet, two-dimensional diffuser models were employed. This simplification permitted the use of powerful optical diagnostic tech-

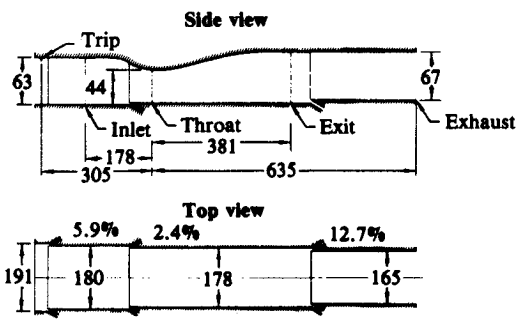

Dimensions in mm.
Vertical dimensions doubled.
Slot sizes enlarged for clarity.
Percentages denote area decrease at slots.

Fig. 1 Diffuser model.

Presented as Paper 84-1636 at the AIAA 17th Fluid Dynamics, Plasmadynamics and Lasers Conference, Snowmass, CO, June 25-27, 1984; received Oct. 29, 1984; revision received May 3, 1985.

*Scientist, McDonnell Douglas Research Laboratories. Senior Member AIAA.

niques and created a flowfield that was within the prediction capability of existing numerical codes. The investigated diffusers did, in fact, exhibit coherent oscillations which are viewed as generically equivalent to those occurring in supersonic inlets.

The diffuser flow oscillations are coherent over the entire subsonic flowfield; the spectra of several fluctuating flow quantities taken at various points all display well-defined peaks at the same frequencies. If the flow is fully attached, then up to three peaks are found, closely corresponding to the natural frequencies predicted by simple one-dimensional acoustic theories.[12,14] The frequencies vary inversely with the goemetric length of the subsonic flowfield within the model.[14] However, if the flow displays shock-induced separation, then only one spectral peak is found, the frequency of which scales with the length of the core flow and does not correspond to acoustic predictions.[14] The mechanisms responsible for these oscillations are known to include convective disturbances, but their current understanding is incomplete.

In addition to the studies of the natural oscillations, investigations into the response of the diffuser flow to periodic downstream perturbations have also been conducted.[15,16] An unexpected result was the lack of any resonance in either the pressure or shock motion when the flow was excited at one of its natural frequencies. The conclusion drawn is that either the mode of oscillation resulting from the excitation differs significantly from the natural mode or that the oscillations are highly damped.[15] Clarification of the lack of resonance in the excited-diffuser studies may indicate the degree to which inlet/combustor coupling could be a practical problem.

The purpose of the present study is to determine the modal structure of the natural oscillations in a separated, supercritical, transonic diffuser flow. The study is motivated by the general desire to better characterize and eventually predict unsteady flows in supersonic inlets, and to clarify the possible differences between the natural and forced oscillations in the diffuser model. To accomplish this task, simultaneous measurements were made of the instantaneous shock location and the subsonic velocity flowfield. In addition, unsteady core pressures from previous work[14,15] were incorporated to form as complete a description as possible of the flowfield oscillations. Since the shock exerts a strong influence on the entire subsonic flow, the shock motion provides a suitable reference for characterizing the coherent contributions to the unsteady velocities and pressures. Therefore, the velocity and pressure data were ensemble-averaged according to the instantaneous shock phase.

Experimental Arrangement

A diagram of the diffuser model used in this study is shown in Fig. 1; it is a converging-diverging channel with an exit-to-throat area ratio of 1.52. The aspect ratio at the throat is 4.05. The top-wall boundary layer is tripped ahead of the converging channel section. Reference 14 presents details of the experimental facility and, together with Ref. 16, describes the unexcited flowfield for this model in terms of shock location, wall and core flow pressures (time-mean and rms fluctuation values), and laser Doppler velocimeter (LDV) measurements of the subsonic flowfield.

The diffuser was operated at a sufficiently high pressure ratio ($p_0/p_{exit} = 1.38$) to cause shock-induced separation in the top-wall boundary layer. At this operating condition, the flow has a natural oscillation frequency of approximately 210 Hz, as determined from shock location and wall and core flow pressure measurements.[14]

A procedure was devised (Fig. 2) to obtain simultaneous measurements of the instantaneous shock location using a line-scan camera,[17,18] and of the subsonic flowfield velocity using a two-component LDV system.

The terminal shock system, shown schematically in Fig. 2, contained a lambda pattern near the top wall, with the separation bubble originating at the foot of the (oblique) upstream leg of the lamba. The shock-imaging camera was trained on the single vertical shock that terminated at the bottom wall. These two parts of the shock system curved smoothly to join at approximately midchannel height and moved as a single unit as the system oscillated. The measured shock-location perturbations were therefore in phase with perturbations imposed on the separation bubble through the shock/boundary-layer interaction. The (normal) downstream leg of the lambda, while moving in phase with the rest of the system, had a slightly larger amplitude, changing the location of the bifurcation point of the lambda pattern throughout the cycle.

The LDV system was operated in a dual-beam, off-axis, forward-scattering configuration. The light source was a 4-W argon-ion laser operated at 488 nm. A Bragg cell was used for measurements in the boundary layers and reversed flow regions. The streamwise and vertical dimensions of the laser probe volume were 0.5 mm each. The receiving optics were offset by 26 deg from the optical axis, providing a spanwise resolution of 0.9 mm. Measurements were made with the beams aligned ±45 deg to the horizontal. To provide an adequate number of scattering particles, the flow was artificially seeded inside the plenum chamber upstream of the model with submicrometer-sized dioctyl phthalate droplets. The photodetector signals (bursts) were analyzed with a commercial counter-type processor.

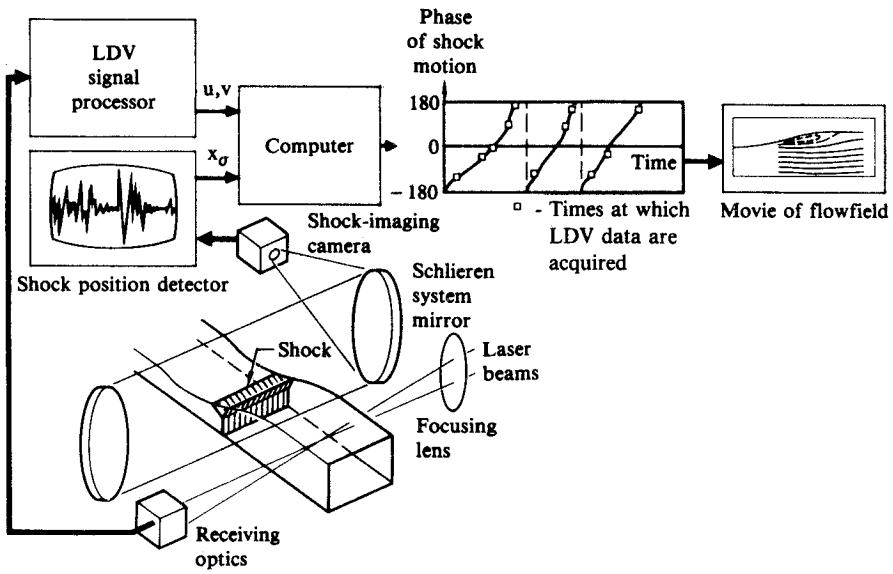

Fig. 2 Data acquisition procedure for a nearly periodic, naturally oscillating, diffuser flowfield.

Two separate, appropriately synchronized, computer-controlled data acquisition systems were employed. One sampled the shock-location information at a fixed rate; and another acquired the velocity information, which became available randomly as seed particles passed through the laser probe volume. A clock on the LDV system interface provided the time intervals between the randomly acquired velocity data points. Since a fixed time interval exists between the individual shock-location data points, concurrent time histories of the shock motion and velocity data could be constructed.

In addition, static and total pressures throughout the core flow were available for both unexcited and excited cases from previous work.[14,15] Pressure measurements were made with miniature, strain-gage transducers that have a flat frequency response up to 90 kHz. The pressure data were recorded on FM tape along with shock-location signals; thus, the same ensemble-averaging procedure applied to the velocity data can be applied to the pressure data as well.

Data Reduction Procedure

The velocity data were sorted and ensemble-averaged according to the instantaneous shock phase. This task was not straightforward because the spectrum of the shock motion (Fig. 3), although containing a well-defined peak at approximately 210 Hz, also contains significant contributions from a relatively wide range of frequencies. In addition, the amplitude of the shock oscillation varies considerably from one cycle to the next. To extract the instantaneous shock phase, numerical techniques involving digital filters and a Hilbert transform were employed.[19,20] These methods have been used successfully in cases with more strictly periodic flow oscillations than those encountered here,[21] and their application in the present situation proved equally successful.

The main features of the procedure for determining the shock phase are shown in Fig. 4. The raw shock-location signal (Fig. 4a) is first bandpass-filtered between 100 and 300 Hz, bracketing the spectral peak. The filtering removes most of the noise (Fig. 4b) but leaves the essential spectral features of the signal intact (Fig. 3). A Hilbert transform is then applied to the filtered data. The effect of the transform is to shift the instantaneous signal phase by 90 deg (Fig. 4c). Every peak in Fig. 4b corresponds to a zero crossing in Fig. 4c, even though the periods and amplitudes of the individual cycles vary considerably. The instantaneous phase (Fig. 4d) is then calculated as the inverse tangent of the quotient of the filtered and transformed signals. At a phase of 0 deg, the shock is passing through its time-mean location, proceeding downstream.

Since a time history of the shock phase now exists, the simultaneously acquired velocity data can be sorted as desired. Fourier analysis of the sorted velocity data provides the amplitude and phase (relative to the shock phase) of the first five harmonics, although only the first harmonic is used for detailed study. An example of the result of the sorting procedure is shown in Fig. 5.

Analysis of the shock-location signal itself yields a mean shock location along the midstream line of $\bar{x}=2.38$ and an amplitude of 0.061 throat-heights.

Two velocity components were acquired at 11 streamwise and 22 vertical locations within the subsonic flowfield, and a detailed map of the flowfield was generated from the 242-point matrices. LDV measurements were made only to 1.5 mm from the bottom wall and 5 mm from the top wall, although closer measurements would have been technically possible. The limitation was imposed by the large disparity between the data rates of the two types of measurements being performed. Shock-position data are acquired at a fixed rate, while LDV burst rates strongly depend on the measurement location within the flowfield. The maximum test time for acquiring shock-position data is limited by the data storage capacity of the system computer. The minimum data acquisition period for LDV data is determined by the minimum number of individual bursts needed to calculate a reliable ensemble average; approximately 4000 samples were used. Near the wall, the LDV data rate is as much as two orders of magnitude less than the core-flow data rate; as a result, the minimum required LDV time exceeds the maximum possible test time for the shock-position measurement system. Reliable simultaneous acquisition of both types of data was, therefore, not possible near the wall. System alterations or the collection of a sufficient number of multiple records at each location were deemed impractical. These limitations, however, did not impede adequate characterization of the flowfield since the dimensions of the velocity fluctuation structures coherent with the shock motion are expected to be of the order of the channel height.

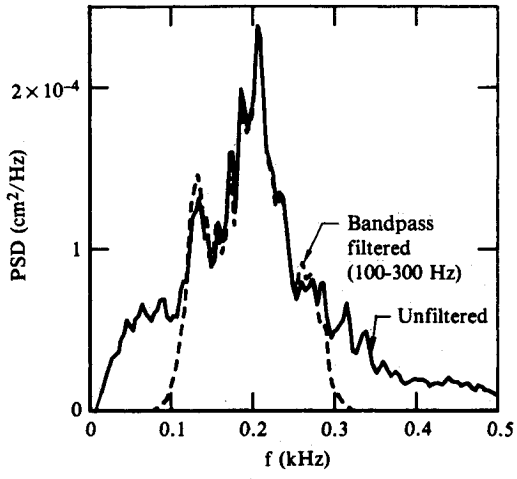

Fig. 3 Power spectral density (PSD) distributions of the self-excited shock motion.

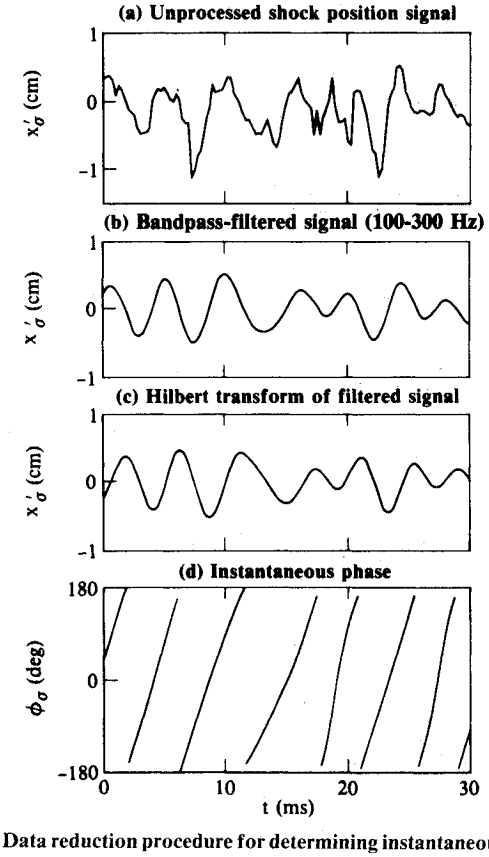

Fig. 4 Data reduction procedure for determining instantaneous shock phase.

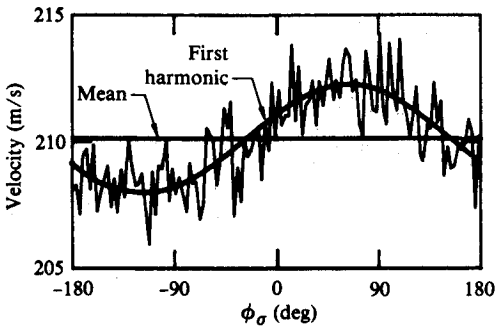

Fig. 5 Example of velocity data ensemble-averaged according to shock phase.

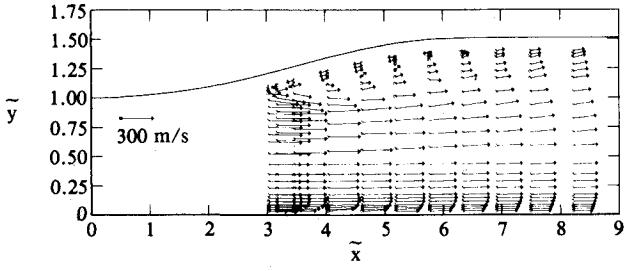

Fig. 6 Time-mean velocity vectors.

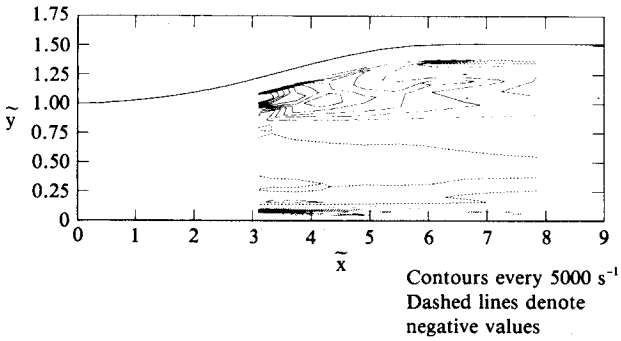

Fig. 7 Contours of time-mean z-component vorticity.

To preserve optical access of the line-scan camera to the shock, LDV measurements could not be made closer than 0.65 throat-heights to the shock.

Velocity Field Results

Figure 6 displays the time-mean velocity vectors. The dominant flow feature is the large region of reverse flow along the top wall resulting from a shock-induced separation. The flow appears to reattach at $\tilde{x} \cong 6$, in excellent agreement with the results of earlier oil-flow measurements.[14] Deflection of the flow around the separation bubble because of the greatly increased local blockage is evident. Reverse velocity magnitudes range as high as 20% of the core-flow velocities.

The time-mean spanwise vorticity field is shown in Fig. 7. The larger thickness and growth rate of the top-wall boundary layer compared to the bottom-wall boundary layer are evident. The maximum positive value attained is 81,000 s^{-1}, occurring near the upstream edge of the separation bubble. The maximum negative value is $-88{,}000$ s^{-1}, occurring at the upstream edge of the measured region, near the bottom wall.

The magnitudes of the ensemble-averaged velocity fluctuations are extremely small. In the core flow, the amplitudes are less than 1% of the mean-flow velocity. In the boundary layers, the coherent fluctuations are more than an order of magnitude smaller than the local turbulence levels, yielding signal-to-noise ratios less than 0.1. A moderate amount of scatter was present in the ensemble-averaged, Fourier-analyzed data, and some smoothing was applied to vertical profiles of the measured amplitudes and phases. Several curve-fitting techniques were tried, none proved satisfactory over the full range of data. Ultimately, a combination of a cubic spline fit and an interpolation technique was employed. Uncertainties in the amplitude measurements were estimated to range from less than 0.5 m/s in the core flow to between 2 and 3 m/s in boundary layers. Uncertainties in the phase measurements ranged from less than 5 deg in the core flow to as much as 30 deg in the top-wall boundary layer downstream of the separation bubble. Nevertheless, a definitive picture of the flow stucture could be determined.

Figure 8a shows a contour plot of the amplitude of the ensemble-averaged streamwise fluctuation. The greatest activity is in the two boundary layers, where fluctuations reach 18 m/s at the edge of the separation bubble, near the shock. The pattern shown in Fig. 8a is qualitatively similar to the pattern of amplitudes determined for the excited flow case[16]; however, the magnitudes for the natural oscillations are less than one-half of the excited values. Only streamwise velocity data were acquired in Ref. 16.

The fact that the largest amplitudes occur in regions where the mean velocity has its steepest gradient suggests that the gross motion is a vertical oscillation of the core flow, causing an oscillation in the boundary-layer thickness. The LDV detects the Eulerian velocity at a fixed location whose distance from the wall corresponds to some fraction of the boundary-layer thickness. This fraction changes as the boundary-layer thickness oscillates, and the velocity associated with this fraction varies according to the shape of the velocity profile. The steeper the gradient, the greater the velocity change for a given change in boundary-layer thickness.

Inspection of the phase contours of the streamwise fluctuations (Fig. 8b) supports the view of a transversely oscillating core flow over a substantial portion of the measured region. The phase difference between the top and bottom of the flow is approximately 180 deg: when one side experiences an acceleration, the other side decelerates. The disturbance propagates normal to constant-phase lines, which are generally horizontal. Again, the pattern shown in Fig. 8b qualitatively resembles the pattern found in excited flows.[16]

One purpose of this study was to determine what differences, if any, exist between the natural and forced oscillation modes in an attempt to explain the lack of resonant behavior when the flow is forced at its natural frequency. The forced oscillations were asymmetrically excited by means of a rotor imbedded in the bottom wall near the diffuser exhaust. Some questions existed whether the asymmetry in the excitation technique is responsible for the transverse oscillation of the core flow, as seen in the velocity field data.[16] It is now evident that a similar mechanism is present in the unexcited flow as well. The amplitude and phase distributions of the streamwise velocity fluctuations show comparable patterns.[16]

The separation bubble appears to be a more effective medium for propagating shock-generated disturbances downstream than the high-speed core flow. In the core flow near the shock, the disturbance propagates in the streamwise direction; the constant-phase lines are generally vertical. The velocity fluctuation farthest upstream in the measured region of the core flow leads the shock by 40 deg (Fig. 8b). That same phase relation exists throughout the entire separation bubble to locations considerably farther downstream. Furthermore, the effects caused by the separation bubble dominate. The shock-location oscillation reflects a shock-strength oscillation. This shock-strength variation causes periodic thickening of the separation bubble which, in turn, causes the boundary-layer pulsation and the attendant vertical core-flow deflection. The streamwise-propagating velocity disturbances in the core flow (indicated by vertical phase lines) are quickly and completely overwhelmed by the transverse, separation-generated motion.

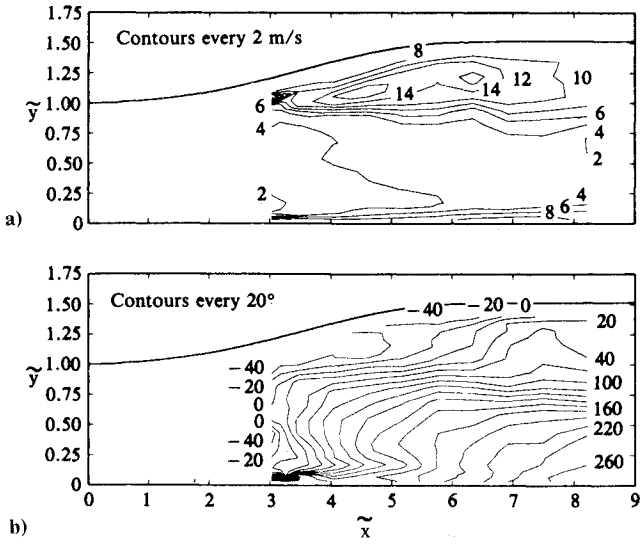

Fig. 8 Contours of ensemble-averaged streamwise velocity fluctuation: a) amplitude and b) phase.

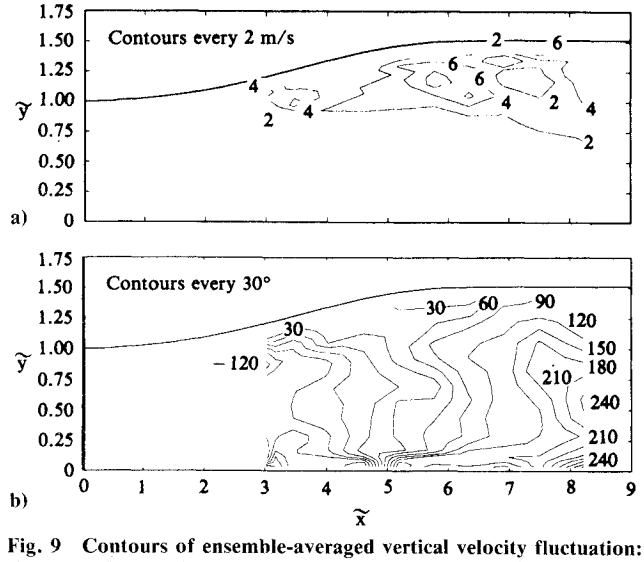

Fig. 9 Contours of ensemble-averaged vertical velocity fluctuation: a) amplitude and b) phase.

The amplitude distribution of the vertical velocity fluctuations is shown in Fig. 9a. The bulk of this activity is confined to the top-wall boundary layer, primarily in the wake of the separation. The magnitudes are considerably smaller than those of the streamwise fluctuations. The location of the greatest vertical fluctuation does not coincide with the location of the greatest streamwise fluctuation, where shear is greatest. Rather, the greatest vertical activity appears to be in regions where the mean flow has its greatest vertical component, excluding the separation bubble itself. It is this region that has been most strongly affected by the presence of the separation. Therefore, it is reasonable that pulsations of the separation bubble would cause the most pronounced variations in the flow direction in this region. The vertical velocity fluctuations arise primarily from oscillations in the total velocity vector angle.

The phase contours of the vertical velocity fluctuations are presented in Fig. 9b. The irregularities in the contours result primarily from the uncertainties in the measurements, as discussed above. Since the LDV velocity component measurements were made by inclining the probe volume ±45 deg to the horizontal, the vertical component involves computing the difference between two (nearly equal-magnitude) measurements, increasing the data scatter. Nevertheless, the contours can be seen as being generally vertical over most of the measured region, indicating a net streamwise propagation of the vertical fluctuations. This pattern is consistent with the existence of a transverse oscillation (flapping) of the core flow, as suggested by the streamwise velocity fluctuation.

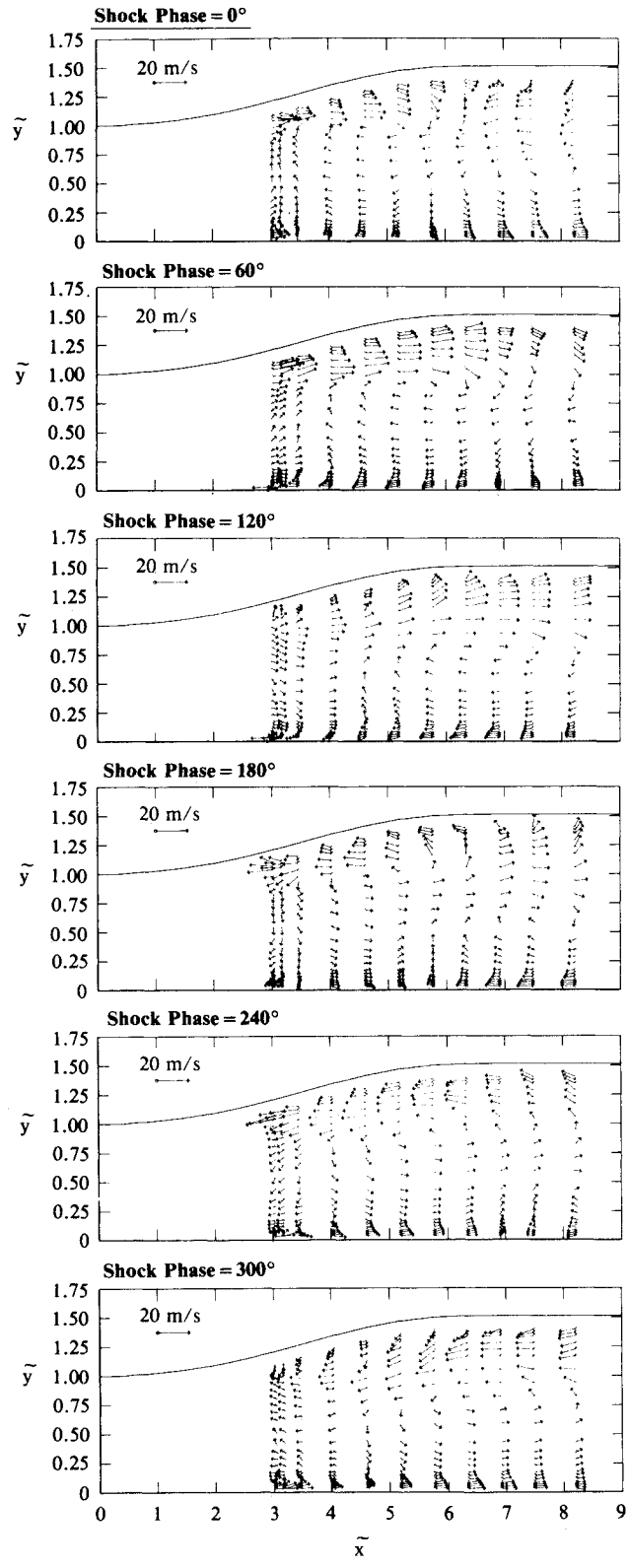

Fig. 10 Temporal development of ensemble-averaged velocity-vector fluctuation.

The phase and amplitude information for the two velocity components can be combined to show the temporal develop-

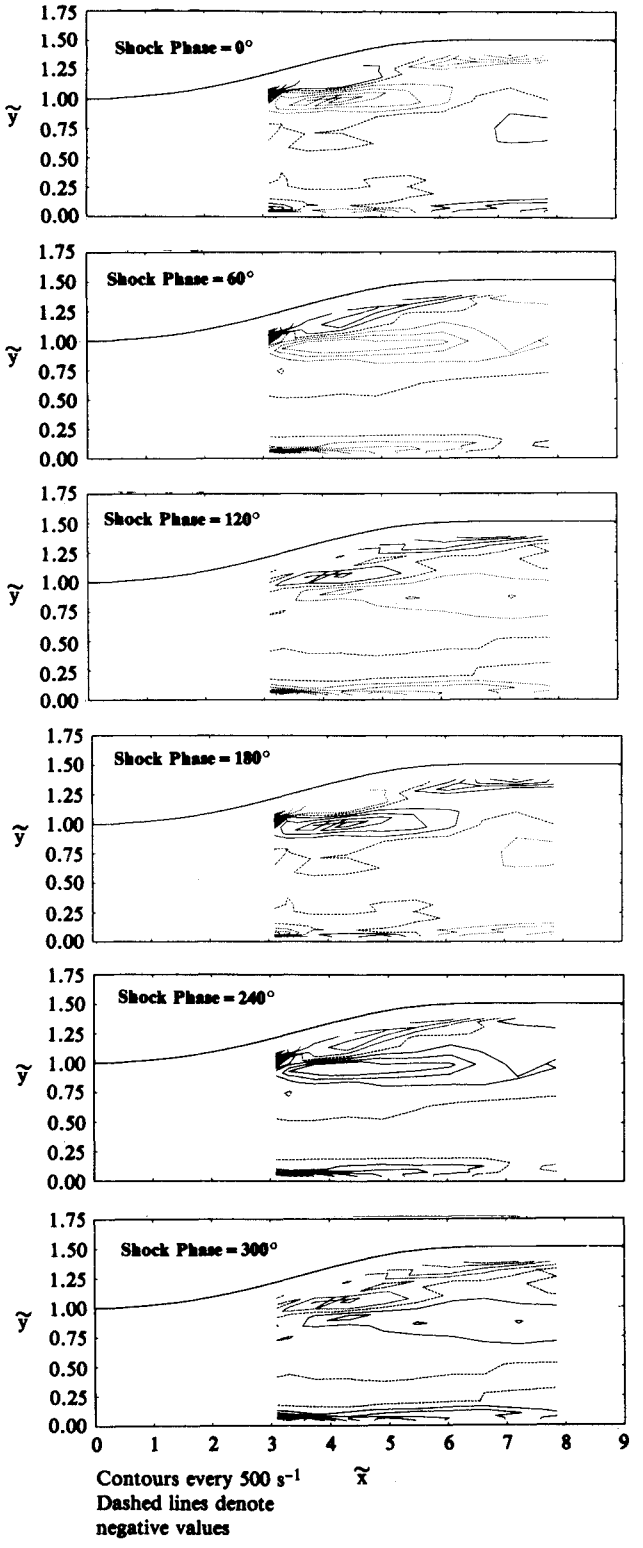

Fig. 11 Temporal development of ensemble-averaged z-component vorticity fluctuation.

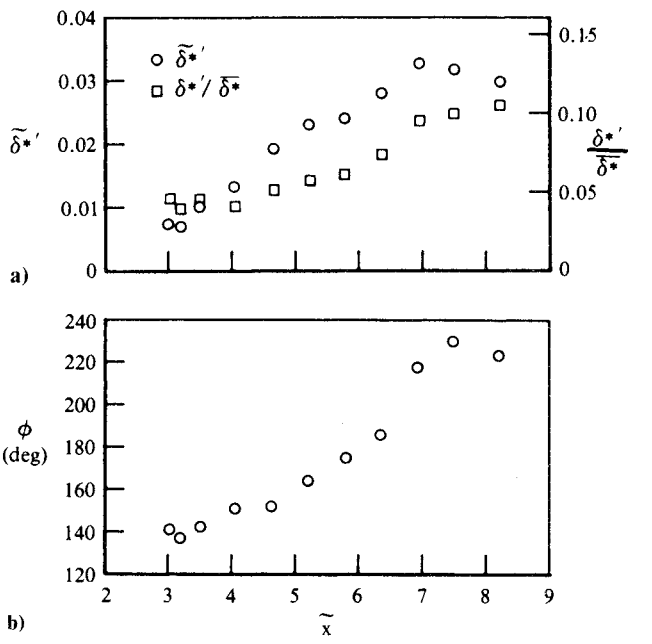

Fig. 12 Ensemble-averaged displacement-thickness fluctuation: a) amplitude and b) phase.

ment of the flowfield. Figure 10 displays the velocity-vector fluctuations as the flow oscillation proceeds through one complete cycle. In this enhanced representation, the fluctuations appear to be organized into a large, rotating structure that is convected downstream, followed by a similar structure rotating in the opposite sense. The center of the structure originates at the edge of the separation bubble and moves toward the bottom wall as it travels downstream. The alternate accelerations and decelerations of the flow on the top and bottom walls, as determined from the one-dimensional representation, are now seen as manifestations of the net rotational motion of a succession of large structures.

The evolution of the z-component vorticity contained in the structures in Fig. 10 is displayed as contour plots in Fig. 11. Each frame in Fig. 11 corresponds to the adjacent frame in Fig. 10. Although the structures seem organized into a coherent rotational motion, the bulk of the vorticity fluctuation remains near the edge of the separation bubble, rather than being convected with the structure. The structures move into the diffuser midstream where the magnitude of the velocity fluctuations is considerably diminished from the magnitudes near the separation bubble and throughout the top-wall boundary layer. Hence, even though there remains an organized rotational motion, the magnitude of the vorticity in the structures decreases. The maximum vorticity magnitude within these structures, 2500 s^{-1}, is located at $\tilde{x}=4.32$, $\tilde{y}=1.00$, and occurs at phases of 15 (negative maximum) and 195 deg (positive maximum). This value is approximately 10% of the local mean vorticity.

In summary, the flowfield proceeds through one complete cycle as follows: As the shock travels downstream and strengthens, it evokes a response in the subsonic flow in two primary areas: in the core flow where the interaction is purely inviscid, and in the top-wall boundary layer where the effects of the shock/boundary-layer interaction dominate.

The strengthening shock in the core flow causes a decrease in the postshock velocity. When the effects of shock velocity are included, it is estimated from acoustic theory[22] that the postshock velocity fluctuation lags the shock-location fluctuation by 110 deg for the flow under investigation. This prediction is a reasonable extrapolation of the measured streamwise velocity fluctuation data along the midstream line.

The increased pressure jump across the strengthening shock caused the boundary layer to thicken. The displacement-thickness-fluctuation amplitude and phase (Fig .12) are taken as quantitative descriptions of the boundary-layer response. Extrapolating the phase (Fig. 12b) back to the location where the upstream leg of the lambda pattern impinges on the top wall ($\tilde{x}=1.98$), the boundary layer is seen to lag the shock by approximately 125 deg. The close agreement of this phase lag with the lag in the core flow, a purely inviscid phenomenon, is not viewed as coincidental; however, the reason for this agreement is not yet clear.

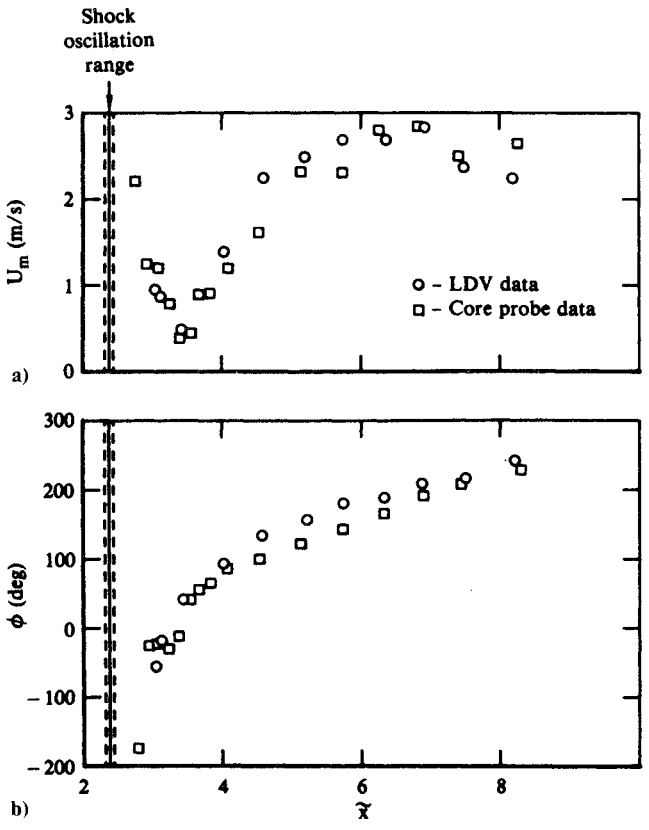

Fig. 13 Emsemble-averaged, natural, streamwise velocity fluctuation along midstream: a) amplitude and b) phase.

The disturbances at the shock described above then propagate downstream. At the upstream-most measurement stations, the displacement thickness reaches a minimum at approximately $\phi = 50$ deg, with the overall flow pattern nearly as seen in the second frame of Fig. 10. The accelerated streamwise velocites at the top wall represent the thinning boundary layer; the velocities are near a maximum at this phase. At this same streamwise location, the streamwise velocity fluctuation in the core flow is nearly in phase with the shock, passing through zero at $\phi = 0$ deg (Fig. 10, frame 1), while the vertical velocity fluctuation, nearly one-quarter cycle ahead, is approaching a maximum. The result is a net upsweep from the core flow translating into forward motion near the top wall. This pattern creates the trailing edge of one of the rotating structures. As the shock passes through one complete cycle, the pair of alternately rotating structures is seen to emerge into the measurement region.

The displacement-thickness-fluctuation amplitude increases both in absolute terms and relative to the local mean displacement thickness (Fig. 12a) as the boundary-layer disturbance propagates downstream, surpassing 10% of the mean value at the end of the measurement region. The manifestation of the boundary-layer-thickness propagation in the separation bubble is to create a pulsation of the bubble, an alternate shortening and thickening, then lengthening and thinning. The pulsations cause a vertical flapping in the core flow, forcing the bottom-wall boundary layer to become thinner as the top-wall boundary layer thickens. As mentioned previously, this transverse motion in the core flow arising from the boundary-layer fluctuation quickly overwhelms the acoustic disturbances originating from the shock.

Related Pressure Field Results

Pressure data were available on FM tape from previous studies of the diffuser model at the same mean-flow conditions.[14,15] These data include fluctuating static and total pressures measured throughout the core flow at $\bar{y} = 0.432$. The instantaneous shock location was recorded with the pressure signals so that the data reduction procedure applied to the velocities could also be applied to the pressures.

The core-pressure and LDV data provide a redundancy by which each measurement can validate the other. Using the method described in Ref. 15, the amplitude and phase of the unexcited streamwise velocity fluctuations were calculated from the amplitudes and phases of the ensemble-averaged unexcited core total and static pressure fluctuations. These data are plotted in Fig. 13 along with the LDV data measured at the same height above the bottom wall, $\bar{y} = 0.432$; the agreement is excellent. A similar calculation was made for pressure and velocity data for flow excited at 300 Hz. It showed the same excellent agreement,[16] lending credence to both the pressure and velocity data.

The velocity-fluctuation amplitude distribution (Fig. 13a) shows the presence of a minimum at $x = 3.5$. Such a feature might suggest the presence of a node in a standing-wave pattern, similar to that in an organ pipe. However, in the conventional standing-wave pattern, the fluctuation phase shows an abrupt 180 deg phase shift as the node is crossed. No such shift is seen in the velocity fluctuation phase (Fig. 13b) at the location of the amplitude minimum. The phase distribution is continuous and monotonically increasing downstream, indicating the presence of a downstream-propagating disturbance as shown in Fig. 10.

Although there is the suggestion of a nodal pattern is the static pressure amplitude distribution, the overall oscillation mode cannot be purely acoustic. If the diffuser is modeled as an organ pipe with a mean flow, a detailed analysis[23] shows that the net amplitude distribution for counterpropagating acoustic wave would present a nodal pattern similar to that displayed in Fig. 13a, but the phase distribution would be that of an upstream-propagating wave.

Reference 23 speculates on the existence of a downstream-traveling "interface wave" in addition to the counterpropagating acoustic waves. As an upstream-traveling acoustic wave impinges on the shock, it produces a reflected acoustic wave shifted by some (frequency-dependent) phase[22]; in addition, the recoil of the shock causes a disturbance in the separated boundary layer which is convected downstream at a speed approximately one half of the core-flow velocity. The LDV data support the existence of such a convected structure for both excited and unexcited flows. The measured pressure and velocity fluctuations are then the resultant of the acoustic and boundary-layer disturbances. Analysis shows that such a combination is capable of generating a nodal pattern in the amplitude distribution, along with a net downstream-propagating phase pattern.[23]

Summary

Simultaneous measurements were made of the subsonic velocity field and shock location in a supercritically operated diffuser with a separated flow along the top wall. The flow contained self-excited oscillations at approximately 210 Hz. The velocity data were ensemble-averaged according to the instantaneous shock phase, and plots of the various fluctuating quantities were presented. In addition, fluctuating core-flow static and total pressures from a previous study were analyzed in a similar manner.

The velocity field shows the presence of a downstream-traveling, rotating structure that originates near the edge of the separation bubble and migrates toward the center of the flow, as it is convected downstream at approximately one-half of the core-flow velocity. The amplitude and phase distribution of the fluctuating streamwise velocity component are qualitatively similar to the distributions for the same flow excited at 300 Hz.

Streamwise velocity fluctuations derived from fluctuating core static and total pressures agree well with the LDV measurements. The velocity fluctuations in the core flow show

the presence of a node-like minimum, but the phase distribution is that of a downstream-propagating disturbance rather than a conventional standing-wave pattern. The observed flow characteristics can be explained by postulating the presence of a convected boundary-layer disturbance in addition to the acoustic disturbance.

Acknowledgments

The author wishes to acknowledge the significant contributions to the completion of this project made by Messrs. A. Seckel and R. Price, and would like to thank Drs. M. Sajben and R.W. Wlezien for many useful discussions. This work was sponsored by the McDonnell Douglas Independent Research and Development program.

References

[1]Martin, A.W., "Propulsion System Flow Stability Program (Dynamic)—Part 1," AFAPL-TR-68-142, 1968.

[2]Ferri, A. and Nucci, L.M., "The Origin of Aerodynamic Instability of Supersonic Inlets at Supercritical Conditions," NACA RM L50K30, Jan. 1951.

[3]Fisher, S.A., Neale, M.C., and Brooks, A.J., "On the Sub-Critical Stability of Variable Ramp Intakes at Mach Numbers Around 2," National Gas Turbine Establishment, England, Rept. ARC-R/M-3711, Feb. 1970.

[4]Clark, W.H., "Static and Dynamic Performance Investigations of Side Dump Ramjet Combustors: Test Summary," Naval Weapons Center, China Lake, CA, NWC TP 6209, Dec. 1980.

[5]Clark, W.H., "Geometric Scale Effects on Combustion Instabilities in a Side Dump Liquid Fuel Ramjet," CPIA Pub. 366, Vol. I, 1982, pp. 595-604.

[6]Schadow, K.C., Crump, J.E., and Blomshield, F.S., "Combustion Instability in a Research Dump Combustor: Inlet Shock Oscillations," CPIA Pub. 347, Vol. III, 1981, pp. 341-356.

[7]Crump, J.E., Schadow, K.C., Blomshield, F.S., and Bicker, C.J., "Combustion Instability in a Research Dump Combustor: Pressure Oscillations," CPIA Pub. 347, Vol. III, 1981, pp. 357-370.

[8]Rogers, T., "Ramjet Inlet/Combustor Pulsation Analysis," Naval Weapons Center, China Lake, CA, NWC TP 6053, Jan. 1980.

[9]Rogers, T., "Ramjet Inlet/Combustor Pulsation Analysis," Naval Weapons Center, China Lake, CA, NWC TP 6155, Feb. 1980.

[10]Sajben, M., Kroutil, J.C., and Chen, C.P., "A High-Speed Schlieren Investigation of Diffuser Flows with Dynamic Distortion," AIAA Paper 77-875, 1977.

[11]Sajben, M., Kroutil, J.C., and Chen, C.P., "Unsteady Transonic Flow in a Two-Dimensional Diffuser," *Unsteady Aerodynamics,* AGARD CP 227, 1977, pp. 13-1 to 13-14.

[12]Chen, C.P., Sajben, M., and Kroutil, J.C., "Shock-Wave Oscillations in a Transonic Diffuser Flow," *AIAA Journal*, Vol. 17, Oct. 1979, pp. 1076-1083.

[13]Sajben, M. and Kroutil, J.C., "Effects of Initial Boundary-Layer Thickness on Transonic Diffuser Flows," *AIAA Journal*, Vol. 19, Nov. 1981, pp. 1386-1393.

[14]Bogar, T.J., Sajben, M., and Kroutil, J.C., "Characteristic Frequencies of Transonic Diffuser Flow Oscillations," *AIAA Journal*, Vol. 21, Sept. 1983, pp. 1232-1240.

[15]Sajben, M., Bogar, T.J., and Kroutil, J.C., "Forced Oscillation Experiments in Supercritical Diffuser Flows," *AIAA Journal*, Vol. 22, April 1984, pp. 465-474.

[16]Salmon, J.T., Bogar, T.J., and Sajben, M., "Laser Doppler Velocimeter Measurements in Unsteady, Separated, Transonic Diffuser Flows," *AIAA Journal*, Vol. 21, Dec. 1983, pp. 1690-1697.

[17]Sajben, M. and Crites, R.C., "Real-Time Optical Measurement of Time-Dependent Shock Position," *AIAA Journal*, Vol. 17, Aug. 1979, pp. 910-912.

[18]Roos, F.W. and Bogar, T.J., "Direct Comparison of Hot-Film Probe and Optical Techniques for Sensing Shock-Wave Motion," *AIAA Journal,* Vol. 20, Aug. 1982, pp. 1071-1076.

[19]Rabiner, L.R. and Gold, B., *Theory and Application of Digital Signal Processing,* Prentice-Hall, Englewood Cliffs, NJ, 1975.

[20]McClellan, J.H., Parks, T.W., and Rabiner, L.R., "FIR Linear Phase Filter Design Program," *Programs for Digital Signal Processing,* IEEE Press, New York, 1979, pp. 5.1-1 to 5.1-13.

[21]Wlezien, R.W. and Way, J.L., "Techniques for the Experimental Investigation of the Near Wake of a Circular Cylinder," *AIAA Journal*, Vol. 17, June 1979, pp. 563-570.

[22]Culick, F.E.C. and Rogers, T., "The Response of Normal Shocks in Diffusers," *AIAA Journal*, Vol. 21, Oct. 1983, pp. 1381-1390.

[23]Sajben, M. and Bogar, T.J., "Unsteady Transonic Flow in a Two-Dimensional Diffuser: Interpretation of Test Results," AFOSR-TR-83-0453, March 1982.